Journal of the Meteorological Society of Japan

EARLY ONLINE RELEASE

The DOI for this manuscript is
DOI:10.2151/jmsj.2022-044
J-STAGE Advance published date: July 14th, 2022
The final manuscript after publication will replace the preliminary version at the above DOI once it is available.

Statistical Characteristics of Summer Season Raindrop Size Distribution in the Western and Central Tianshan Mountains in China

Yong ZENG[1]

Institute of Desert Meteorology, China Meteorological Administration, Urumqi, China
Field Scientific Observation Base of Cloud Precipitation Physics in West Tianshan Mountains, Urumqi, China
Xinjiang Cloud Precipitation Physics and Cloud Water Resources Development Laboratory, Urumqi, China

Lianmei YANG

Institute of Desert Meteorology, China Meteorological Administration, Urumqi, China
Field Scientific Observation Base of Cloud Precipitation Physics in West Tianshan Mountains, Urumqi, China
Xinjiang Cloud Precipitation Physics and Cloud Water Resources Development Laboratory, Urumqi, China

Yushu ZHOU

Laboratory of Cloud-Precipitation Physics and Severe Storms, Institute of Atmospheric Physics, Chinese Academy of Sciences, Beijing, China
College of Earth Science, University of Chinese Academy of Sciences, Beijing, China

Zepeng TONG

Institute of Desert Meteorology, China Meteorological Administration, Urumqi, China
Field Scientific Observation Base of Cloud Precipitation Physics in West Tianshan Mountains, Urumqi, China
Xinjiang Cloud Precipitation Physics and Cloud Water Resources Development Laboratory, Urumqi, China

and

Yufei JIANG

Institute of Desert Meteorology, China Meteorological Administration, Urumqi, China
Field Scientific Observation Base of Cloud Precipitation Physics in West Tianshan Mountains, Urumqi, China
Xinjiang Cloud Precipitation Physics and Cloud Water Resources Development Laboratory, Urumqi, China

July 3, 2022

----

1) Corresponding author: Yong Zeng, Institute of Desert Meteorology, China Meteorological Administration, Urumqi, No. 327, Jianguo Rd., Tianshan District, Urumqi City 830002, China
Email: 15099610397@163.com
Tel: +86-15099610397
Fax: +86-2653634

Abstract

Characteristics of raindrop size distribution (DSD) in summer in the western (Nilek) and central (Urumqi) regions in the Tianshan Mountains of China are studied based on three years of second-generation OTT Particle Size Velocity (Parsivel^2) disdrometer data. The FengYun-2G satellite remote sensing data and the ERA5 reanalysis product are used to reveal the dynamical characteristics associated with summer rainfall in Urumqi and Nilek. The DSD in Nilek is significantly different to that in Urumqi. The concentration of mid-size and large size drops is higher in Nilek than in Urumqi. The DSD characteristics for six rain rate classes and two rain types (convective and stratiform) are studied. It is found that the raindrops in Nilek overall have higher mass-weighted mean diameters (D_m) and lower the logarithm of normalized intercept parameters ($\log_{10} N_w$) than the raindrops in Urumqi, which is true for different rain rates and rain types. Convective clusters in Urumqi are similar to maritime clusters, whereas convective clusters in Nilek are more like continental clusters, according to a classification standard of convective clusters. The radar reflectivity, rain rate relations, and the shape and slope relations for rainfall in Urumqi and Nilek are obviously different. The DSD variability in the two regions may be attributed to differences in convective intensity that are closely related to the specific terrain of the Tianshan Mountains.

Keywords Tianshan Mountains; raindrop size distribution; rainfall rate

1. Introduction

Raindrop size distribution (DSD) information is essential for understanding the cloud microphysical processes (Rosenfeld & Ulbrich, 2003) and improving the algorithms of radar quantitative precipitation estimation (QPE) (Seliga & Bringi, 1976; Ryzhkov & Zrnic, 1995; Chapon et al., 2008). Knowing the DSD variability is of great importance for improving microphysical parameterization schemes of numerical weather prediction models (Milbrandt & Yau, 2005; Zhang et al., 2006). In addition, the DSD also plays an important role in soil erosion studies (Rosewell, 1986; Nanko et al., 2016; Janapati et al., 2019).

DSD varies with climate regime, geographical location and rain type (Ulbrich, 1983; Tokay and Short, 1996; Testud et al., 2001; Bringi et al., 2003; Rosenfeld & Ulbrich, 2003; Zhang et al., 2001, 2003). Bringi et al. (2003) classified the convective clusters into maritime-like and continental-like clusters based on the normalized intercept parameter ($\log_{10} N_w$) and mass-weighted mean diameter (D_m) derived from DSDs over different regimes, and found that D_m of maritime-like cluster is smaller than that of continental-like cluster. Seela et al. (2017) indicated that the DSD of summer rainfall shows a higher D_m and a lower $\log_{10} N_w$ in Taiwan than in Palau，although both Taiwan and Palau are islands located in western Pacific. Thompson et al. (2015) studied the DSDs from two equatorial Indian (Gan) and west Pacific Ocean (Manus) islands, and found that the two sites have similar DSD spectra of liquid water content, median diameter, $\log_{10} N_w$, and other integral rain parameters. Wu et al. (2019) investigated characteristics of summer raindrop size distributions in three typical regions of the western Pacific. They found the largest $\log_{10} N_w$ values in the western West Pacific and the largest D_m values in the southern West Pacific. Rainfall structures in regions of different topographic features (mountains, transitional zones, and plains etc.) in southern France were studied by Zwiebel et al. (2016), who revealed the dependency of DSD on orography. Wu and Liu (2017) studied the characteristics of DSD over the Tibetan Plateau and southern China, and pointed out that the number concentration of raindrops of all sizes over southern China is much higher than that in the Tibetan Plateau for convective rainfall. Comparison of the DSD characteristics at five sites located at five districts of Nanjing during the East Asian rainy season (Pu et al., 2020) indicates that the percentage of total rainfall accounted for by extreme rainfall is significantly higher at Luhe (industrial zone) than at other sites by up to 38%, and the largest $\log_{10} N_w$ value also occurred at Luhe.

The above studies are mainly focused on DSD and rainfall in humid areas, while the research on DSD in arid areas is far less than sufficient. The Tianshan Mountains are about 2500 km long and 300 km wide and composed of a series of tall mountains, intermountain basins and valleys. Located in the arid area in the hinterland of Eurasia with the main body in Xinjiang, China, the Tianshan Mountains are the farthest mountains from the ocean in the world (Sorg et al., 2012). Compared with other regions in central Asia, the Tianshan Mountains have more precipitation and water resources, which makes it known as “the water tower of central Asia” (Chen and Li et al., 2016). Zeng et al. (2020) studied the diurnal variation characteristics of spring DSD in the Tianshan Mountains and found that they are related to precipitation system, valley winds, and solar radiation. A recent study of the characteristics of rainy season DSD in the Tianshan Mountains (Zeng et al., 2021) indicated a clear difference between the DSDs over the Tianshan Mountains and in humid regions of China. However, the DSD during the main precipitation period in summer over the Tianshan Mountains has not been well studied. Moreover, the east-west span of the Tianshan Mountains is pretty large, and it is still unclear whether there are differences in DSD in different areas of the Tianshan Mountains. Therefore, the present study attempts to illustrate the DSD differences in summer between the western (Nilek) and central (Urumqi) regions of the Tianshan Mountains based on three years of disdrometer data. Results of the present study will shed light on the microphysical processes in arid areas. The data and methods are briefly introduced in Section 2. The observational results are illustrated in Section 3. The possible reasons for the difference in DSD characteristics between the two regions are discussed in Section 4. The summary and conclusions are presented in Section 5.

2. Data and Methods

2.1 Observational sites and instruments

The disdrometer data used in the present study were collected at two different regions (Urumqi and Nilek) in the Tianshan Mountains in Northwest China by the second-generation OTT Particle Size Velocity (Parsivel^2) disdrometer manufactured by OTT Hydromet, Germany. Both Urumqi and Nilek are located near the Tianshan Mountains in China, and they represent large urban areas with abundant precipitation, good ecological environment characterized by high vegetation coverage and suitable measurement conditions, and dense human habitation near the Tianshan Mountains. In addition, considering the huge size and complex terrain of the Tianshan Mountains, and the obvious differences in terrain between the western Tianshan Mountains and the central area of the Tianshan Mountains in China, whether there are differences in the characteristics of DSDs need to be further explored. Therefore, we comparatively analyzed DSDs of Urumqi and Nilek in this study. Specifically, Urumqi (935 m asl; 43.78°N, 87.65°E) is located in the central area of the Tianshan Mountains in China with east-west terrain, and Nilek (1105 m asl; 43.80°N, 82.52°E) is located in the western Tianshan Mountains with the trumpet-shaped topography that opens to the west. The two sites are situated at almost the same latitude and have similar altitudes, which facilitates this comparative study. Figure 1 shows the locations of the two observational sites and the topography of the Tianshan Mountains, on the north and south sides of which are the extremely arid Taklimakan Desert and the Gurbantungut Desert. Chen and Li et al. (2017) proposed that the Tianshan Mountains are important for water resource and ecological environment maintenance as well as social and economic development in the arid regions of central Asia. In order to further reveal the DSD variability over the Tianshan Mountains in China, two different regions, i.e., Urumqi and Nilek, are selected for comparative study in this paper.

Parsivel^2 disdrometer can measure the size and fall speed of precipitation particles at the same time (Löffler-Mang, 2000; Tokay et al., 2014), and detailed size and fall speed classification information are described in Yuter et al. (2006). In the past ten years, Parsivel^2 disdrometer has been widely used in the measurement of DSD around the world (e.g., Jaffrain & Berne, 2011; Thurai et al., 2011; B. Chen et al., 2013, 2017; Marzuki et al., 2013; Tokay et al., 2013; Konwar et al., 2014; Wu & Liu, 2017; Wu et al., 2019; Pu et al., 2020; Fu et al., 2020; Zeng et al., 2021; Wang et al., 2021). As proposed by Yuter et al. (2006), when a particle is partially within the measuring area, it may be misidentified as a small particle falling faster than other particles with the observed size, and these spurious particles are called margin fallers. Additionally, strong winds and splashing from raindrops hitting instrument surfaces during heavy rainfall may produce unrealistically large number of slow falling particles (Friedrich et al., 2013). Thus, raindrops with diameters above 8 mm or fall speeds 60% above or below the empirical fall velocity-diameter relation proposed by Atlas et al. (1973) are eliminated following the approach of Jaffrain and Berne (2011) and Friedrich et al. (2013). Considering the terrain height, before quality control, air-density adjustments are made to the fall speed-diameter relationship of Atlas et al. (1973) by multiplying the correction factor (B. Chen et al., 2017; Wang et al., 2021), and the correction factor are 1.036 and 1.043 in Urumqi and Nilek, respectively. At the same time, the first two size classes are discarded because of the low signal-to-noise ratio. Furthermore, 1-min samples with fewer than 10 drops or rainfall rate less than 0.1 mm h^{-1} are also excluded (Tokay et al., 2013). Figure 2 presents the number of drops in different diameter and velocity classes before and after quality control in Urumqi and Nilek, respectively. The fall speeds of raindrops of all sizes that are filtered out are mainly below 4 m s^{-1}, and they are most likely caused by strong winds and splashing, especially in Nilek. Eventually, there are 5219 and 9045 1-min effective DSD samples for Urumqi and Nilek respectively during the summers from 2018 to 2020.

In addition to the data observed by $Parsivel^2$ disdrometer, satellite data from FengYun-2G (FY-2G) (Hui et al., 2016) and reanalysis data from the European Centre for Medium-Range Weather Forecasts (ECMWF) Fifth Reanalysis (ERA5) (Hersbach et al., 2019) are also collected. FY-2G is a geostationary meteorological satellite launched by the China Meteorological Administration. It is located above the equator at the longitude of 105°E, and its black body temperature (TBB) data from the IR window (about 11 micrometers) with 0.1°×0.1° spatial resolution and 1-hr temporal resolution are used in the present study. Meanwhile, convective available potential energy (CAPE), vertical integral water vapor, horizontal wind field near the ground, vertical profiles of temperature, and relative humidity data with 0.125°×0.125° spatial resolution and 1-hr temporal resolution are extracted from ERA5 and analyzed.

2.2 DSD parameters

Based on $Parsivel^2$ disdrometer data, the DSD is calculated by:

$$N(D_i) = \sum_{j=1}^{32} \frac{n_{ij}}{S_{eff}(D_i) \cdot \Delta t \cdot V_j \cdot \Delta D_i} \tag{1}$$

where $N(D_i)$ (m^{-3} mm^{-1}) is the number concentration of raindrops per unit volume per unit diameter interval for raindrop diameter D_i (mm); n_{ij} is the number of raindrops within the size bin i and raindrop terminal velocity bin j; V_j (m s^{-1}) is the fall velocity of class j that range from 0.05 to 20.8 m s^{-1} (Table A2 in Yuter et al. (2006)); Δt (s) is the sampling time, here it is 60 s; and ΔD_i (mm) is the interval of the i-th bin. $S_{eff}(D_i)$ (m^2) is the effective sampling area (Tokay et al., 2014), and the term $S_{eff}(D_i)$ is expressed by:

$$S_{eff}(D_i) = 10^{-6} \times 180 \times (30 - \frac{D_i}{2}) \tag{2}$$

The integral rainfall parameters include rain intensity R (mm h^{-1}), rainwater content W (g m^{-3}), and radar reflectivity factor Z (mm^6 m^{-3}). The equations for their calculations are as follows:

$$R = \frac{6\pi}{10000} \sum_{i=1}^{32} \sum_{j=1}^{32} V_j \cdot N(D_i) \cdot D_i^3 \cdot \Delta D_i \tag{3}$$

$$W = \frac{\pi \rho_w}{6000} \sum_{i=1}^{32} N(D_i) \cdot D_i^3 \cdot \Delta D_i \tag{4}$$

$$Z = \sum_{i=1}^{32} N(D_i) \cdot D_i^6 \cdot \Delta D_i \tag{5}$$

where ρ_w (1 g c m^{-3}) is the density of water.

The three-parameter gamma function is widely used to represent the measured raindrop spectra proposed by Ulbrich (1983), and it is written as:

$$N(D) = N_0 \cdot D^{\mu} \cdot \exp(-\Lambda \cdot D) \tag{6}$$

where N_0 (mm$^{-1-\mu}$ m^{-3}), μ and Λ (mm^{-1}) represent the scale, shape and slope parameters, respectively. The nth-order moment of the drop size distribution is expressed as:

$$M_n = \int_0^{\infty} N(D) \cdot D^n \cdot dD = N_0 \frac{\Gamma(n+1+\mu)}{\Lambda^{n+1+\mu}} \tag{7}$$

The truncated moment method (Ulbrich & Atlas, 1998; Zhang et al., 2003) is implemented to calculate the aforementioned three parameters with the third, fourth, and sixth moments as follows:

$$N_0 = \frac{M_3 \cdot \Lambda^{\mu+4}}{\Gamma(\mu+4)} \tag{8}$$

$$\mu = \frac{11 \cdot G - 8 + \sqrt{G \cdot (G+8)}}{2(1-G)} \tag{9}$$

$$\Lambda = (\mu+4) \cdot \frac{M_3}{M_4} \tag{10}$$

where G is

$$G = \frac{M_4^3}{M_3^2 M_6} \tag{11}$$

To solve the nonindependence problem associated with the parameters in the gamma function of DSD, the normalized gamma distribution that can better represent the raindrop spectrum has been proposed (Willis, 1984; Sempere Torres et al., 1994, 1998; Testud et al., 2001), which is expressed by:

$$N(D) = N_w \cdot f(\mu) \cdot \left(\frac{D}{D_m} \right)^{\mu} \cdot \exp\left[-(4+\mu) \frac{D}{D_m} \right] \tag{12}$$

where N_w (mm^{-1} m^{-3}) is the normalized intercept parameter, and D_m (mm) is the mass-weighted mean diameter. N_w, D_m and $f(\mu)$ are calculated as follows:

$$N_w = \frac{4^4}{\pi \cdot \rho_w} \cdot \frac{10^3 \cdot W}{D_m^4} \tag{13}$$

$$Dm = \frac{\sum_{i=1}^{32} N(Di) \cdot D_i^4 \cdot \Delta Di}{\sum_{i=1}^{32} N(Di) \cdot D_i^3 \cdot \Delta Di} \tag{14}$$

$$f(\mu) = \frac{6 \cdot (4+\mu)^{4+\mu}}{4^4 \cdot \Gamma(4+\mu)} \tag{15}$$

3. Results and Discussion

The variation of the mean raindrop concentration, $N(D_i)$ (m^{-3} mm^{-1}) with raindrop size D (mm) during summer in Urumqi and Nilek are displayed in red and blue color respectively in Figure 3. Throughout this study, raindrops with diameters of 1 to 3 mm are considered as mid-size drops, and drops below and above this range are considered small and large drops, respectively, according to previous studies (Tokay et al., 2008; Krishna et al., 2016; Seela et al., 2017; Janapati et al., 2020). Figure 3 demonstrates that the concentration of mid-size and large raindrops is higher in Nilek compared to that in Urumqi, while the opposite is true for the concentration of small raindrops. Rainfall in Nilek has higher mean R, D_m, and lower N_w than rainfall in Urumqi. A lower concentration of small drops and higher concentration of mid-size and large drops in Nilek result in higher D_m values in Nilek than in Urumqi.

3.1 Raindrop size distribution for different rain rate classes

In order to further determine the differences in DSD between Urumqi and Nilek, DSD observations collected at the two regions are classified into six rain rate classes on the basis of R. The six classes are defined as follows: C1: 0.1-0.5 mm h^{-1}, C2: 0.5-1 mm h^{-1}, C3: 1-2 mm h^{-1}, C4: 2-5 mm h^{-1}, C5: 5-10 mm h^{-1}, C6: ≥ 10 mm h^{-1}. The mean raindrop spectra in the two regions for the six rain rates are shown in Figure 4. Statistics of rainfall corresponding to the six rain rate classes in Urumqi and Nilek are provided in Table 1. For the first two rain rate classes (Figure 4a and 4b; C1: 0.1-0.5, C2: 0.5-1 mm h^{-1}), concentrations of mid-size and large drops are higher in Nilek than in Urumqi. For the middle two rain rate classes (Figure 4c and 4d; C3: 1-2, C4: 2-5 mm h^{-1}), the concentrations of raindrops with diameters greater than 1.3 mm for C3 and 1.6 mm for C4 are higher in Nilek than in Urumqi. Additionally, raindrops with diameters larger than 2.1 mm and 2.3 mm also have higher concentration in Nilek than in Urumqi for the last two rain rate classes (Figure 4e and 4f; C5: 5-10, C6: ≥ 10 mm h^{-1}). Figure 4 clearly shows that even after classifying DSDs into different rain rate classes, mid-size and large drops are more common in Nilek than in Urumqi.

For the convenience to compare the six rain rate classes at a given location, average size spectra for C1 to C6 in Urumqi and Nilek are respectively superimposed on the same plot and results are displayed in Figure 5, which shows that the DSDs in Urumqi and Nilek all have a distinct peak structure, and the spectral width and the concentration of mid-size and large raindrops both increase with increasing rain rate.

The box and whisker plot of variations in D_m and $\log_{10} N_w$ corresponding to different rain rate classes are shown in Figure 6. At both regions, D_m increases with increasing rain rate class (Figure 6a), which is caused by the increase in mid-size and large drops accompanied with larger rain rate. D_m values in Nilek are higher than those in Urumqi due to higher concentrations of mid-size and large drops in Nilek. The mean D_m value varies between 0.88 and 1.61 mm in Urumqi and between 1.10 and 2.38 mm in Nilek. Contrary to D_m, the $\log_{10}N_w$ values are higher in Urumqi than in Nilek (Figure 6b). The mean $\log_{10} N_w$ value varies from 3.46 to 4.02 m^{-3} mm^{-1} in Urumqi and from 2.98 to 3.26 m^{-3} mm^{-1} in Nilek. Moreover, the mean values of Z, W, D_m, and $\log_{10} N_w$ in Urumqi and Nilek corresponding to the six rain rate classes are provided in Table 2.

3.2 DSD variations for stratiform and convective precipitation

Stratiform and convective precipitation are two fundamental types of rainfall in nature with different physical mechanisms for the precipitation formation. The DSD characteristics of the two rainfall types are significantly different (Tokay & Short, 1996; Testud et al., 2001; Bringi et al., 2003; Sharma et al., 2009; Niu et al., 2010). In order to classify precipitation into stratiform and convective types, many researchers have developed different classification schemes based on disdrometer (Tokay & Short, 1996; Testud et al., 2001; Bringi et al., 2003; Ulbrich & Atlas, 2007; B. Chen et al., 2013; Krishna et al., 2016; Wen et al., 2016). In the present study, the classification criteria proposed by Bringi et al. (2003) and B. Chen et al. (2013) are used. Specifically, for at least 10 consecutive 1-min rain samples, the rainfall is determined to be stratiform rainfall if R > 0.5 mm h^{-1} and the standard deviation of $R \leq 1.5$ mm h^{-1}, and the rainfall is determined to be convective if $R \geq 5$ mm h^{-1} and the standard deviation of R > 1.5 mm h^{-1}. Samples that cannot meet the above classification criteria are excluded.

The DSD variations for stratiform and convective precipitation in Urumqi and Nilek are shown in Figure 7. For both regions, a relatively high raindrop concentration can be found for convective precipitation compared to that for stratiform precipitation, which is true for the raindrops of all sizes (Figure 7a, b). In both Urumqi and Nilek, the stratiform regimes have nearly exponential distributions, whereas the convective regimes show a broad distribution, which might be at least partly attributed to the collisional breakup of large drops in convective rainfall (Hu & Srivastava, 1995). To further compare the raindrop concentrations in Urumqi and Nilek for a given rain type, DSDs in both regions for stratiform and convective regimes are respectively presented in Figure 7c and 7d. The two plots show that there are more raindrops with a diameter larger than 1.4 mm in Nilek than in Urumqi for the stratiform regimes, and raindrops with a diameter greater than 2.4 mm have a higher concentration in Nilek compared to that in Urumqi for convective regimes.

To further explore the DSD characteristics for stratiform and convective precipitation in Urumqi and Nilek and compare the results with previous studies, the distributions of the mean D_m and $\log_{10} N_w$ values are displayed in Figure 8. The gray rectangles in Figure 8 are for the continental and maritime convective rainfall clusters and the gray dashed line is the stratiform rainfall line proposed by Bringi et al. (2003). For the rainfall in both regions, convective regimes have higher mean D_m and $\log_{10} N_w$ values than stratiform regimes. In contrast, both stratiform and convective precipitation in Nilek have higher D_m and lower $\log_{10}N_w$ values than that in Urumqi. Comparing results of the present study with that of Bringi et al. (2003) for the convective cluster, it is found that convective DSDs in Urumqi are more similar to the maritime-like cluster, while convective DSDs in Nilek are somewhat similar to the continental-like cluster. The above results suggest that the approach to classify continental and maritime convective rainfall clusters proposed by Bringi et al. (2003) may not be always appropriate for classification of convective precipitation in the region of Tianshan Mountains in China, considering that their classification method is mainly applied to rainfall in North America, Australia and the Pacific region.

Additionally, for stratiform rainfall in both regions, the mean D_m and $\log_{10} N_w$ values appear on the left side of the stratiform rainfall line proposed by Bringi et al. (2003). Bringi et al. (2003) proposed two different microphysical processes that can lead to large D_m and $\log_{10}N_w$ variations in stratiform precipitation, i.e., the melting of large snowflakes that is responsible for larger D_m and smaller $\log_{10} N_w$ values and the melting of tiny graupel or smaller rimed ice particles responsible for smaller D_m and larger $\log_{10} N_w$ values. As shown in Figure 8, stratiform precipitation in Urumqi has smaller D_m and larger $\log_{10} N_w$ values than that in Nilek, implying that stratiform precipitations in Urumqi is associated with tiny graupel or smaller rimed ice particles, whereas stratiform precipitations in Nilek is related to melting of large snowflakes. In addition, the mean values of Z, W, D_m, and $\log_{10} N_w$ for the stratiform and convective regimes in the Urumqi and Nilek are listed in Table 3.

Figure 8 also provides observational results from other regions of China for the purpose to reveal the differences in DSD parameters between monsoon regions and arid regions of China. Compared with rainfall in Nanjing in eastern China (B. Chen et al., 2013), Zhuhai in southern China (Zhang et al., 2019) and Beijing in northern China (Ma et al., 2019), rainfall in Nilek shows a smaller $\log_{10} N_w$ value, while the D_m value in Nilek is larger than that in Beijing and Nanjing and smaller than that in Zhuhai. Rainfall in Urumqi shows a smaller D_m value than those in the other four regions mentioned above, while the $\log_{10} N_w$ value in Urumqi is larger than those in the other four regions except the convective rainfall in Zhuhai. The above results apply to both stratiform and convective rainfall, indicating that the DSD characteristics are different between the monsoon region of China and the arid region of China.

3.3 The D_m-R and N_w-R Relations

Figure 9 shows the scatterplots of D_m and $\log_{10} N_w$ corresponding to different rainfall rates in Urumqi and Nilek. The D_m values in Urumqi are scattered within the range from 0.4 to 2 mm with a few points that have values around 2-2.4 mm (Figure 9a), whereas the D_m values in Nilek are distributed between 0.4 and 3.5 mm with a few points that have values between 3.5 and 4 mm (Figure 9b). In addition, the distribution of D_m narrows and its changes tend to be gentle as the rainfall rate increases for both regions, which could be attributed to the fact that DSDs reach an equilibrium state when the raindrop coalescence and breakup balance each other out at higher rainfall rates (Hu & Srivastava, 1995). The values of $\log_{10}N_w$ in Urumqi are mainly distributed between 2 and 5.1 m^{-3} mm^{-1}, whereas they are mainly scattered from 1.4 to 4.5 m^{-3} mm^{-1} in Nilek. The power law fitting algorithms derived for $D_m - R$ and $\log_{10} N_w - R$ are also presented in Figure 9. Comparing the $D_m - R$ relations at the two places, the coefficient and exponent values are higher in Nilek than in Urumqi. For the $\log_{10} N_w - R$ relations, however, the coefficient value in Nilek is lower than in Urumqi. This indicates that for a given rainfall rate, precipitation in Nilek has higher D_m and lower log N_w values than that in Urumqi, which is consistent with the conclusion shown in Figure 6. In addition, by comparing with the research results of DSDs of typhoon and non-typhoon rainfall observed in Taiwan obtained by Janapati et al. (2021), larger coefficient and exponent values appear in the $D_m - R$ relation of Nilek but not in the two types of rainfall in Taiwan. For the $\log_{10} N_w - R$ relations, the coefficient value of Urumqi is larger and the coefficient value of Nilek is smaller than the two types of rainfall in Taiwan. From the comparison of the two relations between this study and the area between the Yangtze River and Huaihe River in eastern China during summer reported by Jin et al. (2015), it can be seen that Nilek is significantly different from the area between the Yangtze River and Huaihe River, while Urumqi is closed to the area between the Yangtze River and Huaihe River.

3.4 Radar Reflectivity (Z)-Rain Rate (R) Relations

The $Z-R$ relationship ($Z = A \cdot R^b$) plays an important role in QPE of single polarized radar, which heavily depends on the variability of DSD that is related to climate, topography, season, and rainfall type (Tokay & Short, 1996; Atlas et al., 1999; Ulbrich & Atlas, 2007; Chapon et al., 2008; Marzuki et al., 2013). In the $Z = A \cdot R^b$ relationship, the coefficient A is related to the presence of large or small drops, and the exponent b is related to the microphysical process. The collision-coalescence mechanism plays a dominant role in rainfall when b is greater than 1, while the collision-coalescence and break-up process reach equilibrium in homogeneous rainfall when b approaches 1 (Atlas et al., 1999; Atlas and Williams 2003; Steiner et al. 2004; Sharma et al., 2009; Seela et al., 2017; Janapati et al., 2020; Pu et al., 2020). The samples of convective rainfall collected in Urumqi and Nilek are not sufficient and also highly scattered, which makes it hard to fit an appropriate power-law relationship. Therefore, here we mainly focus on the $Z-R$ relationship of stratiform rainfall, which prevails in the two regions. The $Z-R$ relationship ($Z = 200R^{1.6}$) proposed by Marshall and Palmer (1948) has been commonly used in the mid-latitude continental region for stratiform rainfall (hereafter referred to as the MP-Stratiform relationship). Figure 10 shows the scatterplots of Z versus R and the fitted relationships for stratiform precipitation over the two regions. As shown in Figure 10, the $Z-R$ relationship of stratiform rainfall in Nilek has higher coefficient and exponent values than that in Urumqi. The MP-Stratiform relationship is also presented in Figure 10 for comparison. With low radar reflectivity value

($Z < 352.18$ mm^6 m^{-3} (that is, 25.47 dBZ)), the MP-Stratiform relationship would overestimate the precipitation in Urumqi. The opposite is true when the radar reflectivity is high. For the stratiform rainfall in Nilek, the MP-Stratiform relationship would cause overestimation of rainfall. In other words, there are obvious differences in stratiform rainfall between Urumqi and Nilek, and the MP-Stratiform relationship should be used with caution in the two regions.

3.5 The $\mu-\Lambda$ Relations

The $\mu-\Lambda$ relationship provides valuable information for in-depth understanding of DSD characteristics and variability (B. Chen et al., 2013; Zhang et al., 2003). The relationship varies with different climate regimes, rainfall types, and terrains (Cao et al., 2008; Vivekanandan et al., 2004; Zhang et al., 2003; Seela et al., 2018; Tang et al., 2014). Therefore, to enhance our understanding of DSD in arid region, the two regions of the Tianshan Mountains located in the typical arid area of China are selected for the present study. Figure 11 shows the scatterplots of μ and Λ values in Urumqi and Nilek. To estimate the $\mu-\Lambda$ relationship for rainfall in Urumqi and Nilek, the criteria proposed by B. Chen et al. (2017) are adopted in the present study. DSD data are filtered first and only those with total drop counts > 300 are used for further analysis. Zhang et al. (2003) and Cao et al. (2008) pointed out that when μ and Λ are greater than 20 and 20 mm^{-1}, respectively, the results are more likely to be attributed to measurement errors instead of rainfall physics. Therefore, these results are removed from this study. The second-degree polynomial $\mu-\Lambda$

relationships for rainfalls in Urumqi and Nilek are derived respectively and expressed as:

$$\mu = -0.0139\Lambda^2 + 1.0045\Lambda - 2.6141 \quad (16)$$

$$\mu = -0.0139\Lambda^2 + 1.0491\Lambda - 1.7364 \quad (17)$$

Figure 11 clearly shows that the samples of rainfall are more evenly distributed over the entire range in Urumqi, while which are mainly concentrated in the region when μ < 10 and Λ < 10 mm^{-1} in Nilek, meanwhile, it can be seen from the fitted $\mu - \Lambda$ relationship that, given a Λ, Nilek has a larger μ than Urumqi.

The relationship can also be expressed as $\Lambda \cdot D_m = 4 + \mu$ (Ulbrich, 1983). As shown in Figure 11, compared with that in Urumqi, more samples of rainfall in Nilek are located in the higher D_m region, indicating that more higher values of D_m are observed in Nilek than in Urumqi, and this conclusion is consistent with the findings presented in Sections 3.1 and 3.2.

4. Discussion

To explore the possible reasons for the above results in the two regions, the CAPE, vertical integral of water vapor, horizontal wind field near the ground, vertical profiles of temperature, and relative humidity from ERA5 and the TBB from FY-2G in rainy days are calculated for the summers during 2018-2020, in which the statistics are made from data only in rainy days. Figure 12a displays the box and whisker plot of CAPE. It is apparent that the CAPE in Nilek overall is relatively higher than that in Urumqi in rainy days, suggesting that precipitation in

Nilek is more convective than that in Urumqi. Maddox (1980) proposed that TBB can be used as an indicator of convection intensity, and TBB ≤ -32 °C is generally considered to be evidence of convective development. Figure 12b shows that the TBB values are lower in Nilek than in Urumqi in rainy days, indicating that the intensity of convection is stronger in Nilek than in Urumqi, which is closely related the trumpet-shaped topography that opens to the west of the Tianshan Mountains in China for Nilek (Fig. 1). Affected by the topography, prevailing westerly winds in the westerly belt (Zhang & Deng, 1987; Yang et al., 2011; Huang et al., 2017), and the valley winds with diurnal heating (Zeng et al., 2020), airflow is more likely to converge and rise than Urumqi. Further, we compared the DSD characteristics of Nilek in this study with the DSD characteristics of Yining (Zeng et al., 2021) located about 100 km west of Nilek and Xinyuan (Zeng et al., 2020) located about 100 km east of Nilek, and the results showed that summer season DSD in Nilek has the largest mean D_m of 1.37 mm, and the mean D_m of the rainy season DSD in Yining and spring season DSD in Xinyuan are 1.11 mm and 0.92 mm, respectively, and these differences are closely related to the study periods of these three studies, however the effect of different locations on these differences is unknown. Recently, Pu et al. (2020) and Han et al. (2021) used multiple disdrometers to study the DSD characteristics at the regional scale of Nanjing and Beijing, respectively, and found that the DSD characteristics showed differences at the regional scale. Therefore, our future research needs to reveal the regional variability of the DSDs in Nilek, Yining, and Xinyuan based on the observation data in the same time period. At the same time, it is obvious that Nilek have relatively higher vertical integral of water vapor than Urumqi from Figure 13, Combining CAPE, TBB and vertical integral of water vapor in the two regions, it can be inferred that relatively higher water vapor with more active vertical movement leads to the growth of solid and liquid cloud particles to a sufficiently larger size by aggregation, riming, and collision-coalescence processes in Nilek than in Urumqi. Furthermore, average vertical profiles of temperature and relative humidity, and horizontal wind field near the ground for Urumqi and Nilek are shown in Fig. 14 and Fig. 15, respectively. It is obvious that Nilek has relatively higher temperature at all pressure levels (Fig. 14a) and lower relative humidity below 500 hPa (Fig. 14b) than Urumqi. In addition, compared with the more consistent northwesterly wind in Urumqi, the wind direction is more dispersed and the wind speed is stronger in Nilek (Fig. 15). Relative humidity, temperature (Janapati et al., 2020; Seela et al., 2021) and wind (Zeng et al., 2019, Wu et al., 2019) are primary meteorological variables that contribute to evaporation of raindrops. Combining vertical profiles of temperature and relative humidity, and horizontal wind field near the ground in the two regions, it can be inferred that the evaporation processes in Nilek are stronger than in Urumqi, which is a possible reason why Nilek has less number of small drops. The above explanation provides possible reasons for the occurrence of more small drops in Urumqi and more large drops in Nilek. In addition, we also noticed that Nilek has more slow falling particles before quality control as shown in Fig. 2. As Friedrich et al. (2013) proposed, large number of slow falling particles may be produced unrealistically during heavy rainfall. For this study, there are significantly more samples in Nilek (125) than in Urumqi (36) for the last rain rate classes (C6: ≥ 10 mm h^{-1}) as shown in Table 1. Moreover, through the above analysis of CAPE, TBB, and horizontal wind field near the ground, it can be seen that there are stronger convection processes and more scattered strong winds in Nilek, which may be the important reasons for the production of large number of slow falling particles during the process of heavy rainfall in Nilek. Additionally, there are very few margin fallers for both stations before quality control as shown in Fig. 2, which may be related to the improvement of Parsivel^2 disdrometer compared with Parsivel disdrometer (Tokay et al., 2014), the selection of fall speeds 60% above or below the empirical fall velocity-diameter relation proposed by Atlas et al. (1973) after air-density adjustments, or better homogeneity of the laser sheet of Parsivel^2 disdrometer based on more expensive lasers compared to Parsivel disdrometer resulting in improved measurement accuracy (Wen et al., 2017). More possible reasons will be further studied in the future.

5. Summary and Conclusion

In this research, we investigate the characteristics of DSD over the Tianshan Mountains in China using the disdrometer data measured by OTT Pasivel^2 during the summers of 2018-2020. For the first time the characteristics of summer DSD in two different regions (Urumqi and Nilek) of the Tianshan Mountains in China are analyzed. The main conclusions are as follows.

1. Rainfall in Nilek has a higher concentration of mid-size and large raindrops when compared to that in Urumqi. The opposite is true for the concentration of small raindrops. This might be attributed to the fact that convective intensity in Nilek is relatively stronger than that in Urumqi.

2. DSDs are classified into six rain rate classes as well as for stratiform and convective precipitation. Results show a higher concentration of large raindrops and a lower concentration of small raindrops in Nilek than in Urumqi. For all rain rate classes and precipitation types, rainfall in Nilek has a higher mass-weighted mean diameter (D_m) and a lower normalized intercept parameter ($\log_{10} N_w$) than that in Urumqi.

3. Compared with the convective cluster proposed by Bringi et al. (2003), the convective DSDs in Urumqi are more similar to the maritime-like cluster, whereas the convective DSDs in Nilek can be classified as continental-like DSDs (Bringi et al., 2009; Thurai et al., 2010). In addition, D_m and $\log_{10} N_w$ in different regions of China (eastern China, southern China, and northern China) are compared with results in the arid. It is found that the DSD variability is closely related to climate regimes, rainfall types, and terrains.

4. Compared with that in Urumqi, the $Z-R$ relationship for stratiform rainfall in Nilek has higher values of coefficient A and exponent b. The standard $Z-R$ model (MP-Stratiform relationship) tends to overestimate stratiform precipitation in Nilek. For stratiform precipitation in Urumqi, however, the MP-Stratiform relationship would overestimate the precipitation at low radar reflectivity value and underestimate the precipitation at high radar

reflectivity value. In addition, the $\mu-\Lambda$ relations are found to be different between Urumqi and Nilek.

The present study discusses the DSD characteristics and the possible factors affecting these characteristics in the western and central regions over the Tianshan Mountains in China. The results achieved in this study are conducive to the improvement of local quantitative precipitation estimation and a deeper understanding of the DSD characteristic under the background of complex terrain in arid regions. Note that the findings of the present study may be affected by the limitations of the Parsivel^2 disdrometer in measuring small raindrops (Tokay et al, 2013; Zhang et al., 2019). The two-dimensional video disdrometer combined with other observation instruments should be used to further study the microphysical processes that involve cloud droplets and raindrops over the Tianshan Mountains in China in the future.

Data Availability Statement

The ERA5 reanalysis data provided by ECMWF are available at https://www.ecmwf.int/en/forecasts/datasets/, and the TBB data provided by China National Satellite Meteorological Center can be downloaded from http://satellite.nsmc.org.cn. The DSD data generated and analyzed in this study are available from the corresponding author on reasonable request.

Acknowledgments

This work was supported by Tianshan Mountains Talent Project (grant 2021-32), the National Key Research and Development Program of China (grant 2018YFC1507102 and 2018YFC1507104), and Uygur Autonomous Region Tianchi Project for Introducing High-Level Talents (2019). We acknowledge China National Satellite Meteorological Center and ECMWF for providing the data.

References

Atlas, D., C. W. Ulbrich, F. D. Jr. Marks, E. Amitai, and C. R. Williams, 1999: Systematic variation of drop size and radar-rainfall relations. *Journal of Geophysical Research*, 104 (D6), 6155–6169.

Bringi, V., V. Chandrasekar, J. Hubbert, E. Gorgucci, W. L. Randeu, and M. Schoenhuber, 2003: Raindrop size distribution in different climatic regimes from disdrometer and dual-polarized radar analysis. *Journal of the Atmospheric Sciences*, 60(2), 354–365.

Cao, Q., G. Zhang, E. Brandes, T. Schuur, A. Ryzhkov, and K. Ikeda, 2008: Analysis of video disdrometer and polarimetric radar data to characterize rain microphysics in Oklahoma. *Journal of Applied Meteorology and Climatology*, 47 (8), 2238–2255.

Chapon, B., G. Delrieu, M. Gosset, and B. Boudevillain, 2008: Variability of raindrop size distribution and its effect on the Z–R relationship: A case study for intense Mediterranean rainfall. *Atmospheric Research*, 87(1), 52–65.

Chen, B., J. Yang, and J. Pu, 2013: Statistical characteristics of raindrop size distribution in the Meiyu season observed in eastern China. *Journal of the Meteorological Society of Japan*, 91 (2), 215–227.

Chen, B., Z. Hu, L. Liu, G. Zhang, 2017: Raindrop size distribution measurements at 4,500 m on the Tibetan Plateau during TIPEX-III. *Journal of Geophysical Research: Atmospheres*, 122 (20), 11092–12006.

Chen, Y., W. Li, H. Deng, G. Fang, and Z. Li, 2016: Changes in Central Asia's Water Tower: Past, present and future. Scientific Reports, 6, 35458.

Chen, Y., Z. Li, G. Fang, and H. Deng, 2017: Impact climate change on water resources in the Tianshan Mountains, Central Asia. *Acta Geographica Sinica*, 72(1), 18-26.

Fu, Z., X. Dong, L. Zhou, W. Cui, J. Wang, R. Wan, L. Leng, and B. Xi, 2020: Statistical characteristics of raindrop size distributions and parameters in Central China during the Meiyu seasons. *Journal of Geophysical Research: Atmospheres*, 125, e2019JD031954.

Friedrich, K., S. Higgins, F. J. Masters, and C. R. Lopez, 2013: Articulating and stationary PARSIVEL disdrometer measurements in conditions with strong winds and heavy rainfall. *Journal of Atmospheric and Oceanic Technology*, 30 (9), 2063–2080.

Hersbach, H., B. Bell, P. Berrisford, A. Horányi, J. Muñoz Sabater, J. Nicolas, R. Radu, D. Schepers, A. Simmons, C. Soci, and D. Dee, 2019: Global reanalysis: goodbye era-interim, hello era5. *ECMWF Newsletter*, 159, 17-24.

Hu, Z., and R. C. Srivastava, 1995: Evolution of raindrop size distribution by coalescence, breakup, and evaporation: Theory and observation. *Journal of the Atmospheric Sciences*, 52 (10), 1761–1783.

Hui, W., Q., Guo, Q. Wu, L. Yang, 2016: Image quality evaluation of FY-2G meteorological satellite. *Progress in Geophysics*, 31 (5), 1902-1910.

Han, Y., J. P. Guo, Y. X. Yun, J. Li, X. R. Guo, Y. M. Lv, D. Wang, L. Li, and Y. Zhang, 2021: Regional variability of summertime raindrop size distribution from a network of disdrometers in Beijing. *Atmospheric Research*, 257, 105591.

Huang, W., S. Chang, and C. Xie, 2017: Moisture sources of extreme summer precipitation events in North Xinjiang and their relationship with atmospheric circulation. *Adv. Clim. Chang. Res.*, 8, 12-17.

Jaffrain, J., and A. Berne, 2011: Experimental quantification of the sampling uncertainty associated with measurements from PARSIVEL disdrometers. *Journal of Hydrometeorology*, 12 (3), 352–370.

Janapati, J., B. K. Seela, P. -L. Lin, P. -K. Wang, C.-H. Tseng, K. K. Reddy, H. Hashiguchi, L. Feng, S. K. Das, and C. K. Unnikrishnan, 2020: Raindrop size distribution characteristics of Indian and Pacific Ocean tropical cyclones observed at India and Taiwan sites. *Journal of the Meteorological Society of Japan*, 98, 299–317.

Janapati, J., B. K. Seela, P.-L. Lin, P. K. Wang, U. Kumar, 2019: An assessment of tropical cyclones rainfall erosivity for Taiwan. *Scientific Reports*, 9, 15862.

Janapati, J., B. K. Seela, P. -L. Lin, M. -T. Lee, E. Joseph, 2021: Microphysical features of typhoon and non-typhoon rainfall observed in Taiwan, an island in the northwestern Pacific. *Hydrology and Earth System Sciences*, 25, 4025-4040.

Jin, Q., Y. Yuan, H. J. Liu, C. E. Shi, J. B. Li, 2015: Analysis of microphysical characteristics of the raindrop spectrum over the area between the Yangtze River and the Huaihe River during summer. *Acta Meteorol. Sin.*, 73, 778-788. (In Chinese)

Konwar, M., S. K. Das, S. M. Deshpande, K. Chakravarty, and B. N. Goswami, 2014: Microphysics of clouds and rain over the Western Ghat. *Journal of Geophysical Research: Atmospheres*, 119 (10), 6140–6159.

Krishna, U. V. M., K. K. Reddy, B. K. Seela, R. Shirooka, P. -L. Lin, and C. -J. Pan, 2016: Raindrop size distribution of easterly and westerly monsoon precipitation observed over Palau islands in the Western Pacific Ocean. *Atmospheric Research*, 174, 41–51.

Löffler-Mang, M., and J. Joss, 2000: An optical disdrometer for measuring size and velocity of hydrometeors. *Journal of Atmospheric and Oceanic Technology*, 17 (2), 130–139.

Maddox, R. A., 1980: Mesoscale convective complexes. *Bulletin of the American Meteorological Society*, 61(11), 1374-1387.

Marzuki, M., H. Hashiguchi, M. K. Yamamoto, S. Mori, and M. D. Yamanaka, 2013: Regional variability of raindrop size distribution over Indonesia. *Annales Geophysicae*, 31(11), 1941–1948.

McVicar, T. M., M. L. Roderick, R. J. Donohue, L. T. Li, T. G. Van Niel, and A. Thomas, 2012: Global review and synthesis of trends in observed terrestrial near-surface wind speeds: Implications for evaporation. *Journal of Hydrology*, 416-417, 182-205.

Milbrandt, J. A., and M. K. Yau, 2005: A multimoment bulk microphysics parameterization. Part I: Analysis of the role of the spectral shape parameter. *Journal of the Atmospheric Sciences*, 62(9), 3051–3064.

Nanko, K., S. M. Moskalski, and R. Torres, 2016: Rainfall erosivity–intensity relationships for normal rainfall events and a tropical cyclone on the US southeast coast. *Journal of Hydrology*, 534, 440–450.

Niu, S., X. Jia, J. Sang, X. Liu, C. Lu, and Y. Liu, 2010: Distributions of raindrop sizes and fall velocities in a semiarid plateau climate: Convective versus stratiform rains. *Journal of Applied Meteorology and Climatology*, 49 (4), 632–645.

Pu, K., X. Liu, Y. Wu, S. Hu, L. Liu, and T. Gao, 2020: A comparison study of raindrop size distribution among five sites at the urban scale during the East Asian rainy season. *Journal of Hydrology*, 590, 125500.

Rosenfeld, D., and C. W. Ulbrich, 2003: Cloud microphysical properties, processes, and rainfall estimation opportunities. *Meteorological Monographs*, 30(52), 237–258.

Rosewell, C. J., 1986: Rainfall kinetic energy in Eastern Australia. *Journal of Climate and Applied Meteorology*, 25(11), 1695–1701.

Ryzhkov, A. V., and D. S Zrnic, 1995: Comparison of dual polarization radar estimators of rain. *Journal of Atmospheric and Oceanic Technology*, 12(2), 249–256.

Seela, B. K., J. Janapati, P. -L. Lin, K. K. Reddy, R. Shirooka, and P. K. Wang, 2017: A comparison study of summer season raindrop size distribution between Palau and Taiwan, two islands in western Pacific. *Journal of Geophysical Research: Atmospheres*, 122, 11,787–11,805.

Seela, B. K., J. Janapati, P. -L. Lin, P. K. Wang, and M. -T. Lee, 2018: Raindrop size distribution characteristics of summer and winter season rainfall over north Taiwan. *Journal of Geophysical Research: Atmospheres*, 123, 11602–11624.

Seela, B. K., J. Janapati, C. Kalath Unnikrishnan, P. -L. Lin, J. L. Loh, W. -Y. Chang, U. Kumar, K. K. Reddy, D. -I. Lee, and M. V. Reddy, 2021: Raindrop size distributions of North Indian Ocean tropical cyclones observed at the coastal and inland stations in South India. *Remote Sens.*, 13, 3178.

Seliga, T. A., and V. N. Bringi, 1976: Potential use of the radar differential reflectivity measurements at orthogonal polarizations for measuring precipitation. *Journal of Applied Meteorology*, 15(1), 69–76.

Sempere Torres, D., J. M. Porrà, and J. D. Creutin, 1994: A general formulation for raindrop size distribution. *Journal of Applied Meteorology*, 33, 1494–1502.

Sempere Torres, D., J. M. Porrà, & J. D. Creutin, 1998: Experimental evidence of a general description for raindrop size distribution properties. *Journal of Geophysical Research*, 103, 1785–1797.

Sharma, S., M. Konwar, D. K. Sarma, M. C. R. Kalapureddy, and A. R. Jain, 2009: Characteristics of rain integral parameters during tropical convective, transition and stratiform rain at Gadanki and its application in rain retrieval. *Journal of Applied Meteorology and Climatology*, 48 (6), 1245–1266.

Sorg, A., T. Bolch, and M. Stoffel, 2012: Climate change impacts on glaciers and runoff in Tien Shan (Central Asia). *Nature Climate Change*, 2(10), 725-731.

Tang, Q., H. Xiao, C. Guo, and L. Feng, 2014: Characteristics of the raindrop size distributions and their retrieved polarimetric radar parameters in northern and southern China. *Atmospheric Research*, 135, 59–75.

Testud, J., S. Oury, P. Amayenc, and R. A. Black, 2001: The concept of “normalized” distributions to describe raindrop spectra: A tool for cloud physics and cloud remote sensing. *Journal of Applied Meteorology*, 40(6), 1118–1140.

Thompson, E. J., S. A. Rutledge, B. Dolan, and M. Thurai, 2015: Drop size distributions and radar observations of convective and stratiform rain over the equatorial Indian and west Pacific Oceans. *J. Atmos. Sci.*, 72(11), 4091–4125.

Thurai, M., W. A. Petersen, A. Tokay, C. Schultz, and P. Gatlin, 2011: Drop size distribution comparisons between Parsivel and 2-D video disdrometers. *Advances in Geosciences*, 30, 3–9.

Tokay, A., and D. A. Short, 1996: Evidence from tropical raindrop spectra of the origin of rain from stratiform versus convective clouds. *Journal of Applied Meteorology*, 35(3), 355–371.

Tokay, A., P. G. Bashor, E. Habib, and T. Kasparis, 2008: Raindrop size distribution measurements in tropical cyclones. *Monthly Weather Review*, 136 (5), 1669–1685.

Tokay, A., W. A. Petersen, P. Gatlin, and M. Wingo, 2013: Comparison of raindrop size distribution measurements by collocated disdrometers. *Journal of Atmospheric and Oceanic Technology*, 30 (8), 1672–1690.

Tokay, A., D. B. Wolff, and W. A. Petersen, 2014: Evaluation of the new version of the laser-optical disdrometer, OTT Parsivel^2. *Journal of Atmospheric and Oceanic Technology*, 31 (6), 1276–1288.

Ulbrich, C. W., 1983: Natural variations in the analytical form of the raindrop size distribution. *Journal of Climate and Applied Meteorology*, 22(10), 1764–1775.

Ulbrich, C. W., and D. Atlas, 1998: Rainfall microphysics and radar properties: Analysis methods for drop size spectra. *Journal of Applied Meteorology*, 37, 912–923.

Ulbrich, C. W., and D. Atlas, 2007: Microphysics of raindrop size spectra: Tropical continental and maritime storms. *Journal of Applied Meteorology and Climatology*, 46 (11), 1777–1791.

Vivekanandan, J., G., Zhang, and E. Brandes, 2004: Polarimetric radar estimators based on a constrained gamma drop size distribution model. *Journal of Applied Meteorology*, 43 (2), 217–230.

Wang, G., R. Zhou, S. Zhaxi, and S. Liu, 2021: Raindrop size distribution measurements on the Southeast Tibetan Plateau during the STEP project. *Atmospheric Research*, 249, 105311.

Wen, L., K. Zhao, G. Zhang, M. Xue, B. Zhou, S. Liu, and X. Chen, 2016: Statistical characteristics of raindrop size distributions observed in East China during the Asian summer monsoon season using 2-D video disdrometer and Micro Rain Radar data: DSD observed in East China. *Journal of Geophysical Research: Atmospheres*, 121, 2265–2282.

Wen, L., K. Zhao, G. F. Zhang, S. Liu, and G. Chen, 2017: Impacts of instrument limitations on estimated raindrop size distribution, radar parameters, and model microphysics during Mei-Yu season in East China. *Journal of Atmospheric and Oceanic Technology*, 34(5): 1021-1037.

Willis, P. T., 1984: Functional fits to some observed drop size distributions and parameterization of rain. *Journal of the Atmospheric Sciences*, 41, 1648–1661.

Wu, Y., and L. Liu, 2017: Statistical characteristics of raindrop size distribution in the Tibetan Plateau and southern China. *Advances in Atmospheric Sciences*, 34 (6), 727–736.

Wu, Z., Y. Zhang, L. Zhang, H. Lei, Y. Xie, L. Wen, and J. Yang, 2019: Characteristics of summer season raindrop size distribution in three typical regions of western Pacific. *Journal of Geophysical Research: Atmospheres*, 124, 4054–4073.

Yuter, S. E., D. E. Kingsmill, L. B. Nance, and M. Löffler-Mang, 2006: Observations of precipitation size and fall speed characteristics within coexisting rain and wet snow. *Journal of Applied Meteorology*, 45 (10), 1450–1464.

Yang, L., X. Li, and G. Zhang, 2011: Some advances and problems in the study of heavy rain in Xinjiang. *Climatic and Environmental Research*, 16(2): 188-198 (in Chinese).

Zeng, Q. W., Y. Zhang, H. C. Lei, Y. Q. Xie, T. C. Gao, L. F. Zhang, C. M. Wang, and Y. B. Huang, 2019: Microphysical characteristics of precipitation during pre-monsoon, monsoon, and post-monsoon periods over the South China Sea. *Adv. Atmos. Sci.*, 36(10), 1103−1120.

Zeng, Y., L. Yang, Z. Zhang, Z. Tong, J. Li, F. Liu, J. Zhang, and Y. Jiang, 2020: Characteristics of clouds and raindrop size distribution in Xinjiang, using cloud radar datasets and a disdrometer, *Atmosphere*, 11 (12), 1382.

Zeng, Y., L. Yang, Z. Tong, Y. Jiang, Z. Zhang, J. Zhang, Y. Zhou, J. Li, F. Liu, and J. Liu, 2021: Statistical characteristics of raindrop size distribution during rainy seasons in Northwest China. *Advances in Meteorology*, 6667786, 1-12.

Zhang, A., J. Hu, S. Chen, D. Hu, Z. Liang, C. Huang, L. Xiao, C. Min, and H. Li, 2019: Statistical characteristics of raindrop size distribution in the monsoon season observed in southern China. *Remote Sensing*, 11 (4), 432.

Zhang, G., J. Vivekanandan, and E. Brandes, 2001: A method for estimating rain rate and drop size distribution from polarimetric radar measurements. *IEEE Transactions on Geoscience and Remote Sensing*, 39, 830–841.

Zhang, G., J. Vivekanandan, E. Brandes, R. Meneghini, and T. Kozu, 2003: The shape-slope relation in observed gamma raindrop size distributions: Statistical error or useful information? *Journal of Atmospheric and Oceanic Technology*, 20, 1106–1119.

Zhang, G., J. Sun, and E. Brandes, 2006: Improving parameterization of rain microphysics with disdrometer and radar observations. *Journal of the Atmospheric Sciences*, 63(4), 1273–1290.

Zhang, J., and Z. Deng, 1987: A Generality of Rainfall in Xinjiang. Meteorological Press, Beijing, China (in Chinese).

Zwiebel, J., J. Van Baelen, S. Anquetin, Y. Pointin, and B. Boudevillain, 2016: Impacts of orography and rain intensity on rainfall structure. The case of the HyMeX IOP7a event. Quarterly Journal of the Royal Meteorological Society, 142 (10), 310–319.

List of Figures

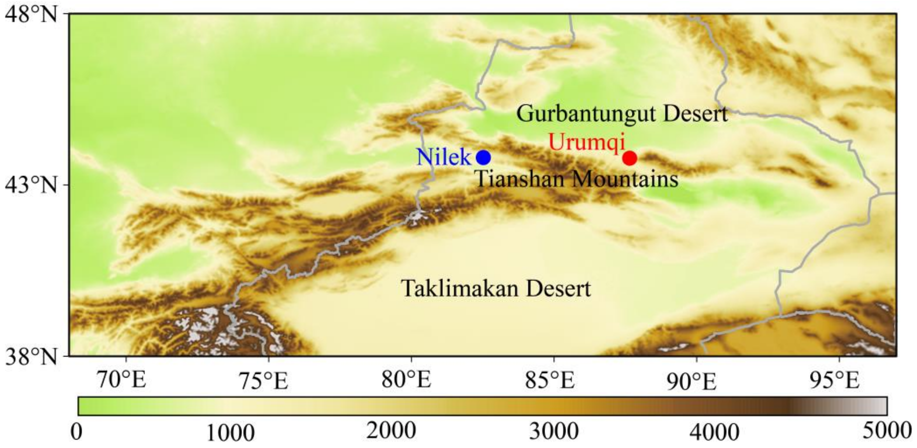

Fig. 1 Locations of the observation sites (the blue and red dot) and the topography (m) of Tianshan Mountains.

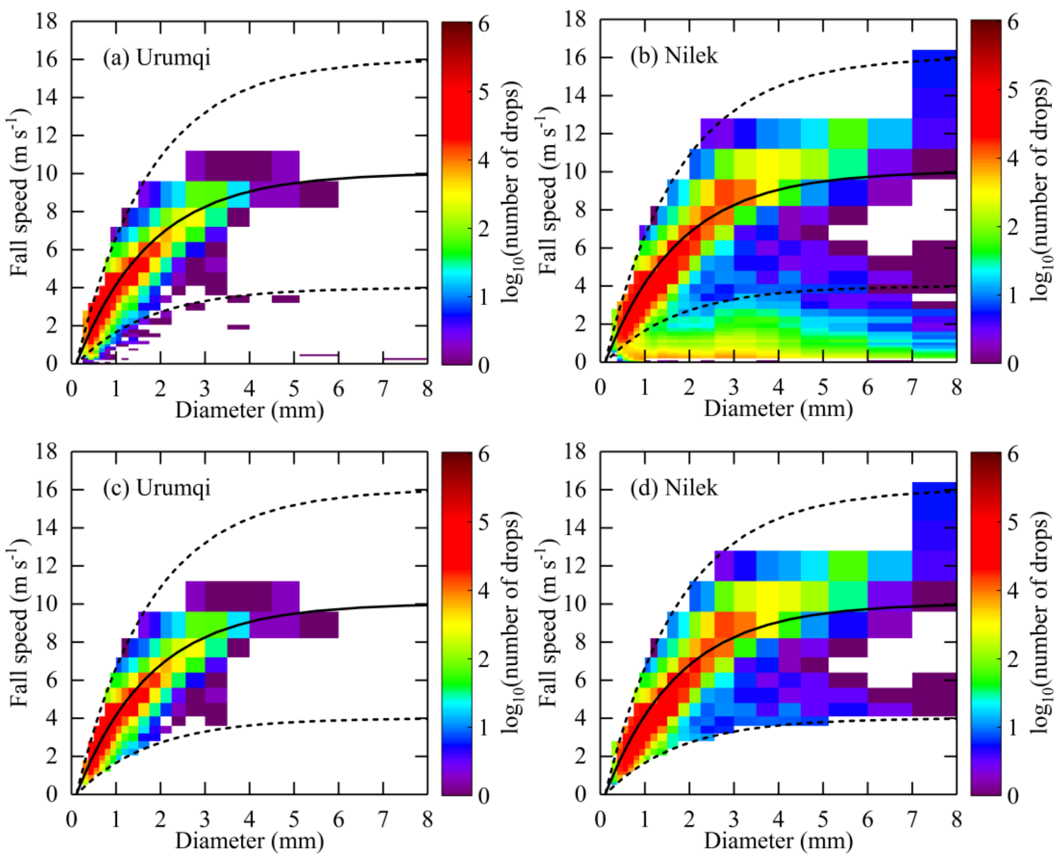

Fig. 2 Raindrop numbers in different diameter and fall speed classes before (a) and (b), and after (c) and (d) quality control in Urumqi and Nilek. The black solid line indicates the empirical fall speed-diameter relationship from Atlas et al. (1973), and the black

dashed line indicates the ± 60 % range of the relationship.

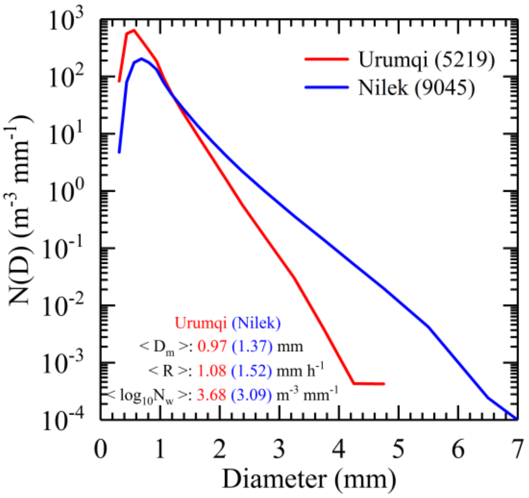

Fig. 3 Mean raindrop concentrations in Urumqi and Nilek during summer. The total numbers of 1-min raindrop size distributions samples in Urumqi and Nilek are given by legends in parenthesis. The mean values (enclosed in angle bracket < >) of mass-weighted mean diameter (D_m, mm), rainfall rate (R, mm h^{-1}) and the normalized intercept parameter ($\log_{10} N_w$, mm^{-1} m^{-3}) for rainfall in Urumqi and Nilek are also shown in Figure 3.

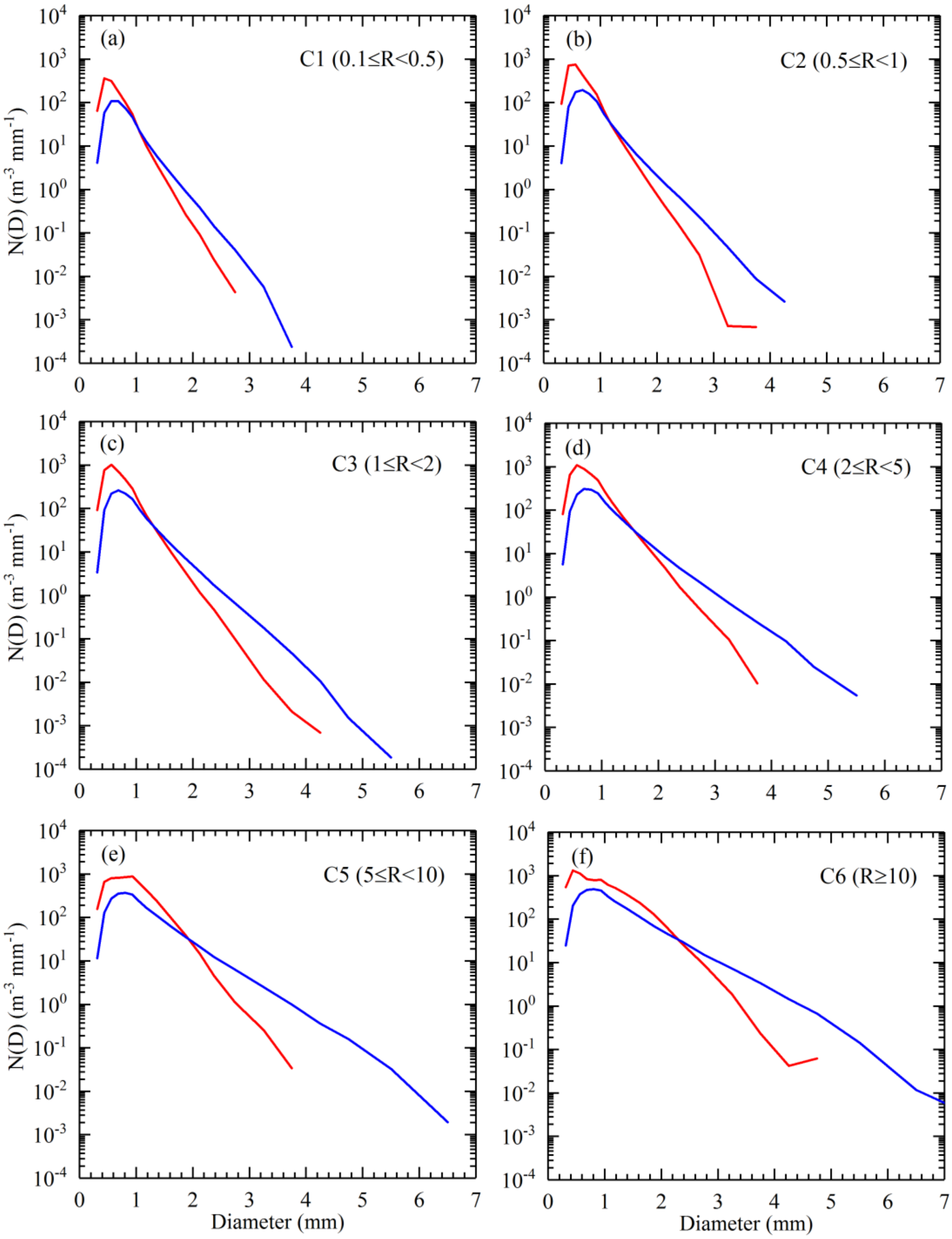

Fig. 4 Average raindrop spectra in Urumqi (red color) and Nilek (blue color) corresponding to six rain rate classes (C1: 0.1–0.5, C2: 0.5–1, C3: 1–2, C4: 2–5, C5: 5–10, C6: ≥ 10 mm h^{-1}).

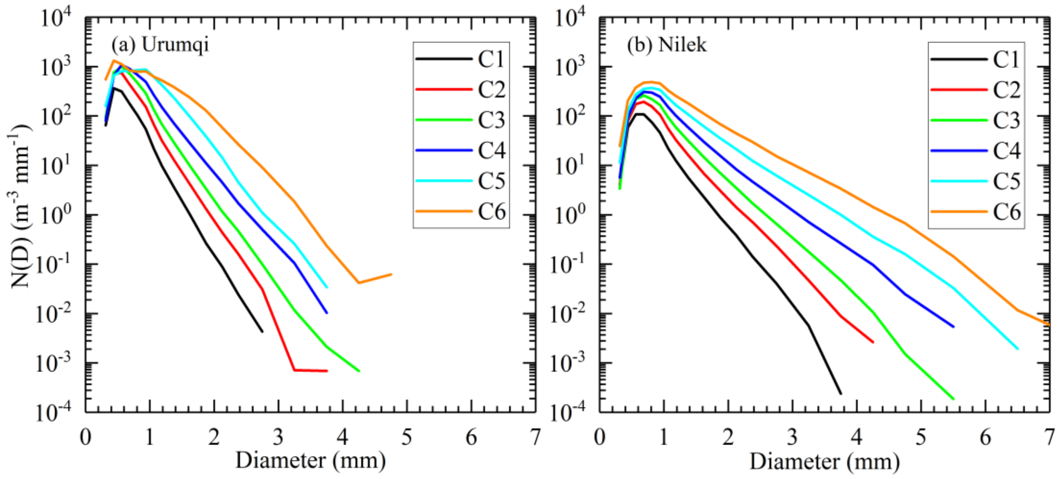

Fig. 5 Average raindrop spectra in Urumqi (a) and Nilek (b) corresponding to six rain rate classes.

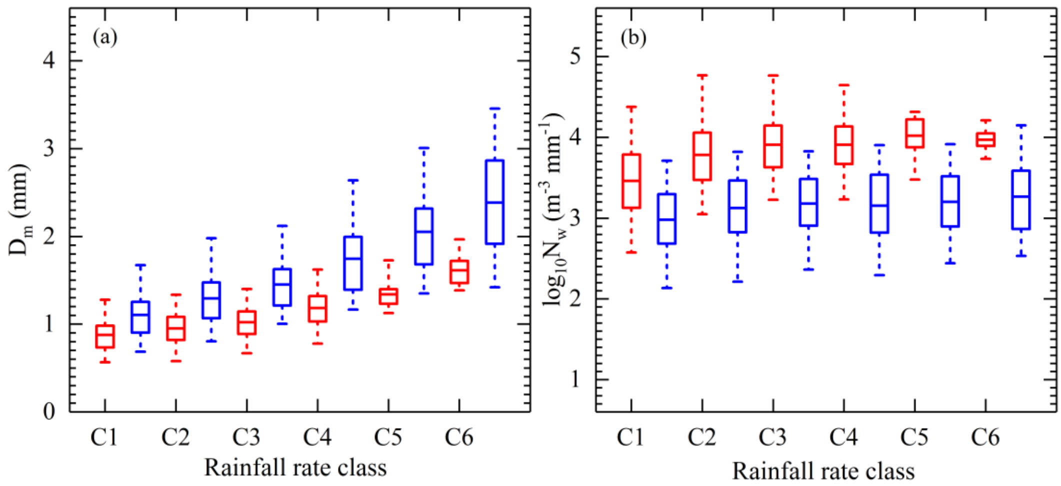

Fig. 6 Variations of the mass-weighted mean diameter (D_m, mm) (a) and the normalized intercept parameter ($\log_{10} N_w$, mm^{-1} m^{-3}) (b) in Urumqi (red) and Nilek (blue) corresponding to six rain rate classes. The central line of the box indicates the median, and the bottom and top lines of the box indicate the 25th and 75th percentiles, respectively. The bottom and top lines of the vertical lines out of the box indicate the 5th and 95th percentiles, respectively.

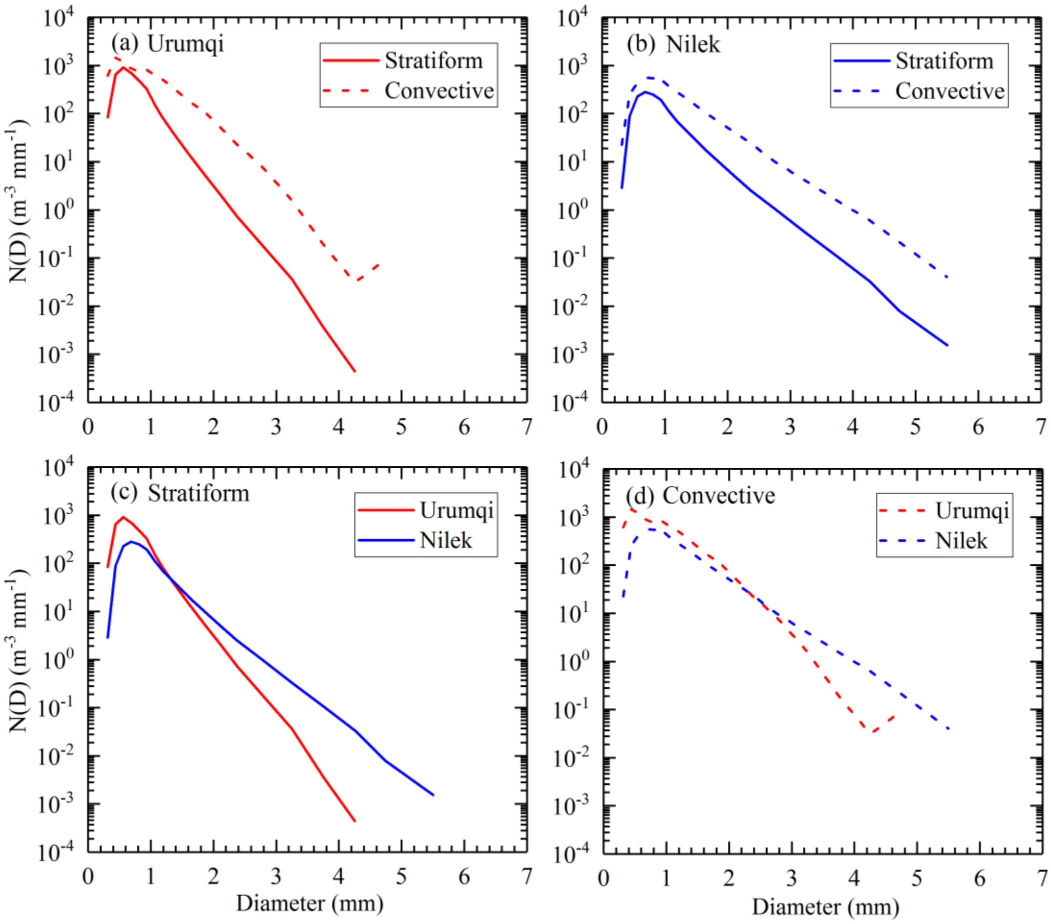

Fig. 7 Variations of raindrop concentration with drop diameter for different precipitation types in Urumqi (red) and Nilek (blue).

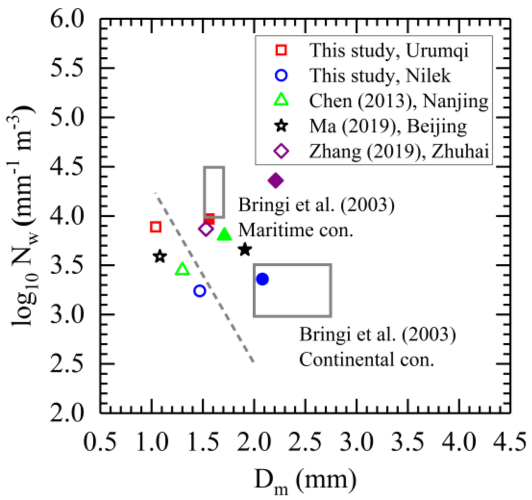

Fig. 8 Scatterplots of the mean value of normalized intercept parameter ($\log_{10} N_w$, mm^{-1} m^{-3}) versus the mass-weighted mean diameter (D_m, mm) for convective rainfall and

stratiform rainfall, where the hollow (solid) symbol corresponds to stratiform (convective) rainfall. The red squares and blue circles represent the mean values in Urumqi and Nilek, respectively. The two grey rectangles correspond to the maritime and continental convective clusters, and the grey dashed line is the stratiform rain line reported by Bringi et al. (2003). The green triangles, black stars, and purple diamonds represent the mean values obtained in previous studies by B. Chen et al. (2013), Ma et al. (2019), and Zhang et al. (2019), respectively.

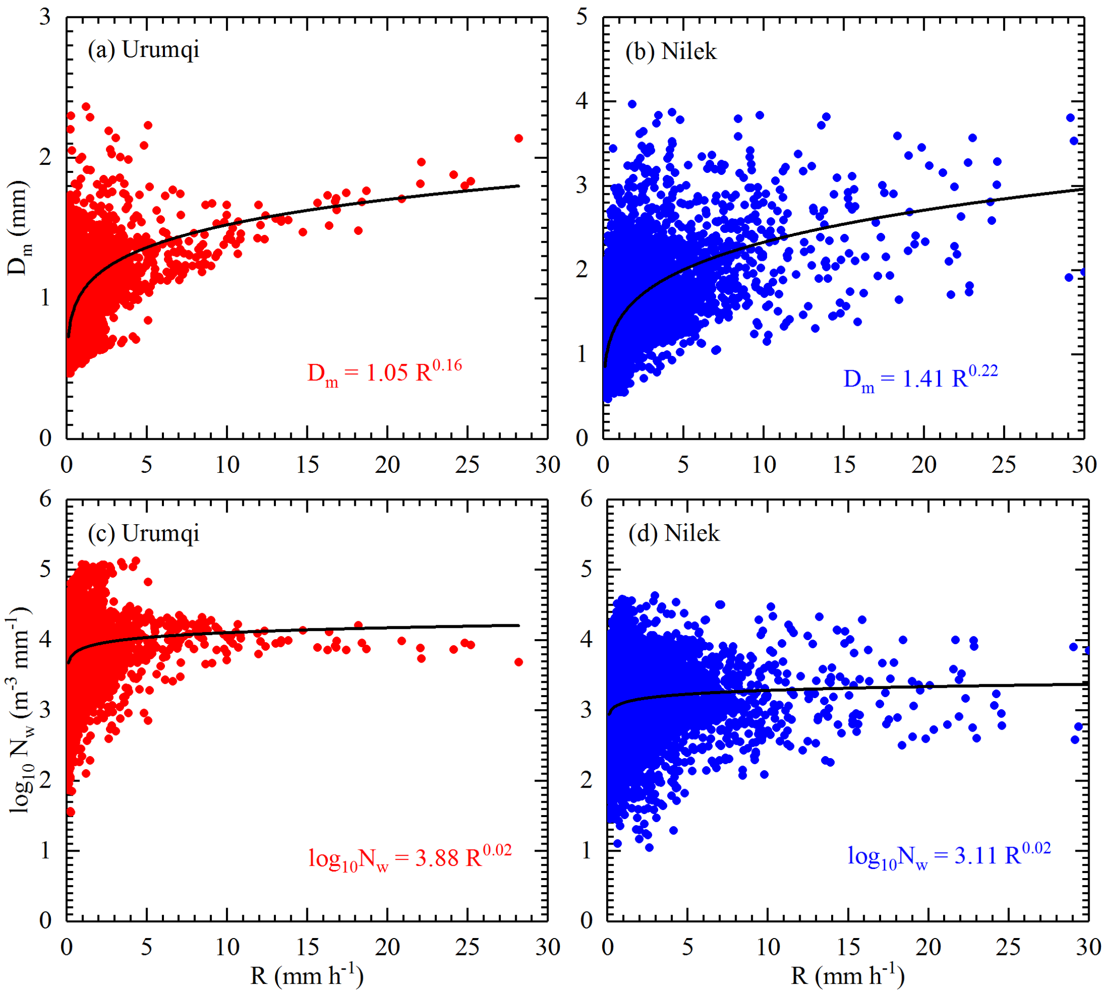

Fig. 9 Scatterplots of the mass-weighted mean diameter (D_m, mm) and the normalized intercept parameter ($\log_{10} N_w$, mm^{-1} m^{-3}) with rainfall rate in Urumqi (red) and Nilek

(blue). The fitted power law relationships are shown by black solid lines. (a) $D_m - R$ relation and (c) $\log_{10} N_w - R$ relation for rainfall in Urumqi; (b) $D_m - R$ relation and (d) $\log_{10} N_w - R$ relation for rainfall in Nilek.

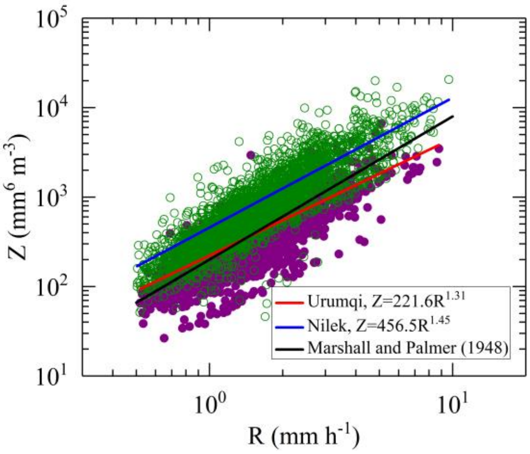

Fig. 10 Scatterplots of radar reflectivity (Z, mm^6 m^{-3}) and rain intensity (R, mm h^{-1}) for stratiform rainfall in Urumqi (purple solid circles) and Nilek (green hollow circles). The fitted power law relationships are shown by the red line (for Urumqi) and blue line (for Nilek), respectively, and the black line indicates the empirical relationship ($Z = 200R^{1.6}$) proposed by Marshall and Palmer (1948).

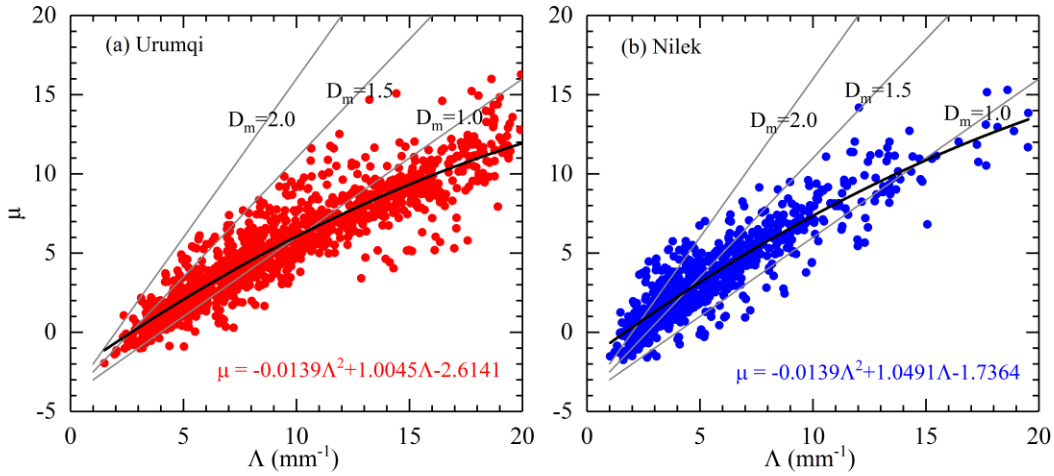

Fig. 11 Scatterplots of $\mu - \Lambda$ relationships and fitting curves for rainfall in Urumqi (a) and Nilek (b) with drop counts > 300. The gray lines correspond to the relationship

$\Lambda \cdot D_m = 4 + \mu$ given the values of D_m = 1.0, 1.5, and 2.0 mm.

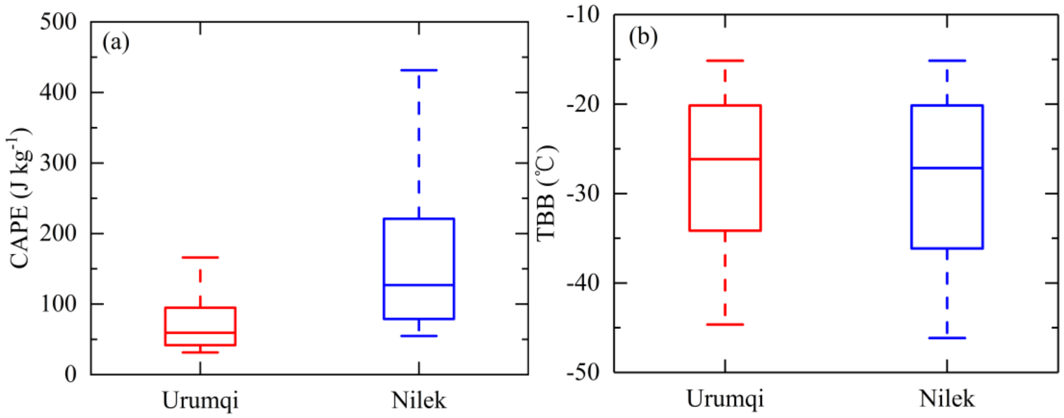

Fig. 12 Box and whisker plots of (a) convective available potential energy (CAPE, J Kg^{-1}) and (b) black body temperature (TBB, °C) in Urumqi (red color box) and Nilek (blue color box). The center line of each box indicates the median value, and the bottom and top lines of the box indicate the 25th and 75th percentiles, respectively. The bottom and top of the dashed vertical lines indicate the 5th and 95th percentiles, respectively.

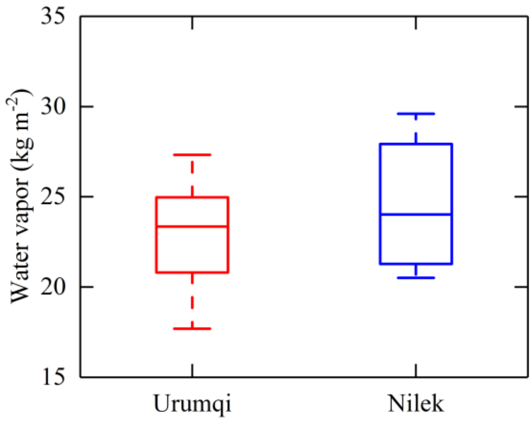

Fig. 13 Box and whisker plots of vertical integral of water vapor (kg m^{-2}) in Urumqi (red color box) and Nilek (blue color box).

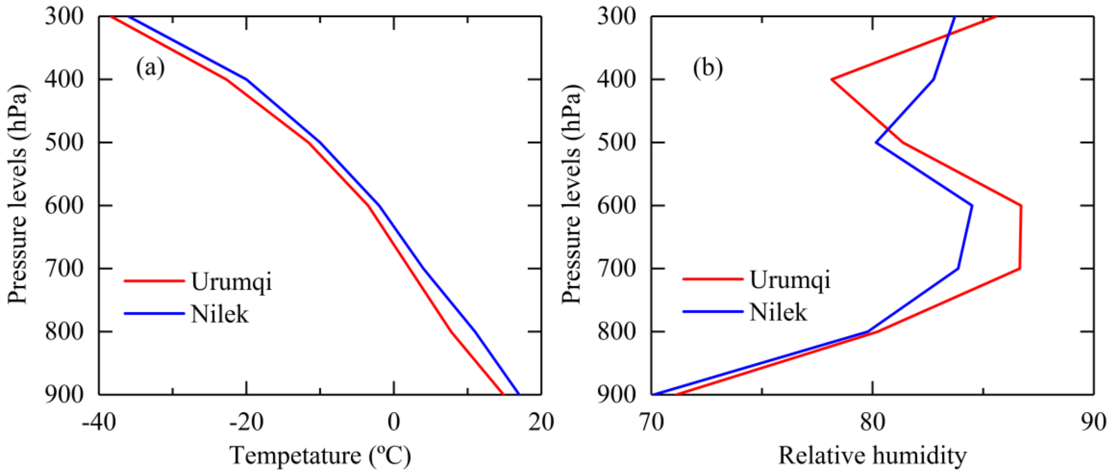

Fig. 14 Mean air temperature (◦C) and (b) relative humidity (%) profiles in Urumqi (red) and Nilek (blue).

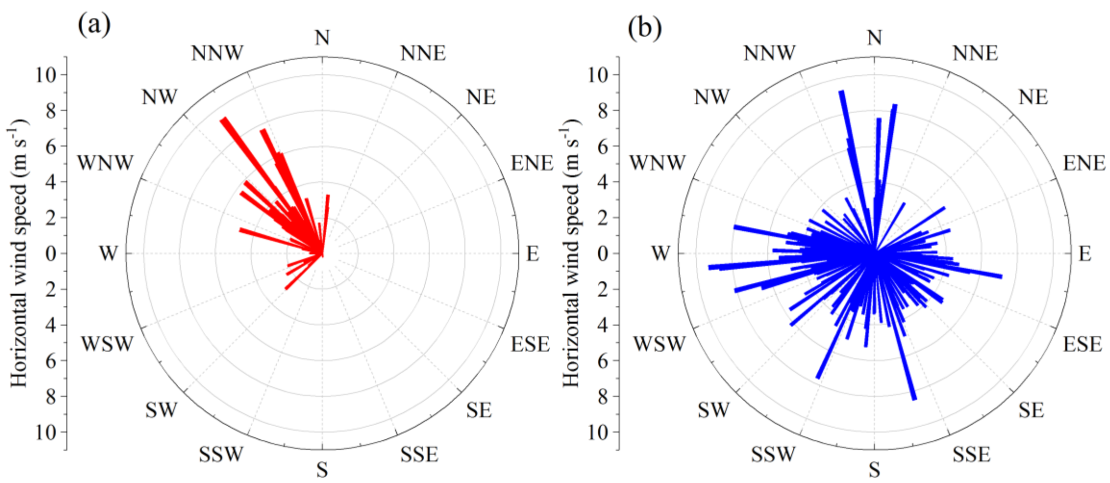

Fig. 15 Wind rose map of the ground in (a) Urumqi and (b) Nilek.

List of Tables

Table 1. Statistics of rainfall in Urumqi and Nilek corresponding to six rain rate classes

Rain rate class	Rain rate threshold (mm h^{-1})	Urumqi			Nilek		
		No. of samples	Mean (mm h^{-1})	SD (mm h^{-1})	No. of samples	Mean (mm h^{-1})	SD (mm h^{-1})
C1	$0.1 \leqslant R < 0.5$	2361	0.25	0.11	3224	0.27	0.11
C2	$0.5 \leqslant R < 1$	1120	0.73	0.14	2001	0.73	0.15
C3	$1 \leqslant R < 2$	1092	1.40	0.27	1964	1.42	0.28
C4	$2 \leqslant R < 5$	520	2.86	0.73	1353	3.01	0.82
C5	$5 \leqslant R < 10$	90	7.01	1.42	378	6.89	1.38
C6	$R \geqslant 10$	36	15.62	4.98	125	15.67	5.35
Total		5219	1.08	1.74	9045	1.52	2.37

Note. SD represents the standard deviation.

Table 2. Mean Values of Z, W, D_m, and $\log_{10} N_w$ in Urumqi and Nilek corresponding to six rain rate classes

Rain rate class	Urumqi				Nilek			
	Z (dBZ)	W (g m^{-3})	D_m (mm)	$\log_{10} N_w$ (m^{-3} mm^{-1})	Z (dBZ)	W (g m^{-3})	D_m (mm)	$\log_{10} N_w$ (m^{-3} mm^{-1})

C1	14.34	0.021	0.88	3.46	17.16	0.017	1.10	2.98
C2	20.40	0.057	0.95	3.78	23.47	0.042	1.29	3.12
C3	24.12	0.102	1.02	3.91	27.76	0.077	1.45	3.18
C4	28.72	0.184	1.18	3.91	32.84	0.150	1.75	3.15
C5	33.69	0.403	1.34	4.02	38.14	0.314	2.05	3.20
C6	39.15	0.780	1.61	3.97	42.81	0.660	2.38	3.26
Total	19.62	0.074	0.97	3.68	24.43	0.077	1.37	3.09

Table 3. Same as Table 2 but for stratiform and convective rain types

Rain type	Urumqi				Nilek			
	Z (dBZ)	W (g m^{-3})	D_m (mm)	$\log_{10} N_w$ (m^{-3} mm^{-1})	Z (dBZ)	W (g m^{-3})	D_m (mm)	$\log_{10} N_w$ (m^{-3} mm^{-1})
Stratiform	24.65	0.115	1.04	3.89	28.59	0.099	1.47	3.24
Convective	38.14	0.688	1.56	3.97	40.15	0.536	2.08	3.36